IEEE Access
Multidisciplinary | Rapid Review | Open Access Journal

Received 24 July 2022, accepted 7 August 2022, date of publication 16 August 2022, date of current version 25 August 2022.

Digital Object Identifier 10.1109/ACCESS.2022.3198945

RESEARCH ARTICLE

Power-Hardware-in-the-Loop Emulation of the Low-Frequency Oscillation Phenomenon in AC Railway Networks

PAUL FRUTOS-GALARZA[1], (Student Member, IEEE), JUAN M. GUERRERO[1], (Senior Member, IEEE), IKER MUNIATEGUI-ASPIAZU[2], IBAN VICENTE-MAKAZAGA[2], AITOR ENDEMAÑO-ISASI[2], DAVID ORTEGA-RODRIGUEZ[2], AND FERNANDO BRIZ[1], (Senior Member, IEEE)

[1]Department of Electrical, Computer and System Engineering, University of Oviedo, 33204 Gijón, Spain
[2]Traction Research and Development Department, Ingeteam Power Technology S.A., 48170 Zamudio, Spain

Corresponding author: Paul Frutos-Galarza (frutospaul@uniovi.es)

This work was supported in part by the European Commission H2020 under Grant UE-18-POWER2POWER-826417; in part by the Spanish Ministry of Science, Innovation and Universities under Grant MCIU-19-PCI2019-103490; and in part by the Government of Asturias under Project AYUD/2021/50988.

ABSTRACT Dynamic interactions among the AC railway traction network and power electronics converters feeding the trains have been reported to cause low-frequency oscillations (LFO) of the catenary voltage and current. This can result in railway system instability, eventually leading to a power outage and the shutdown of the train traffic. To avoid LFO, control of train power electronic converters must be properly designed and tuned. Experimental verification of control performance regarding the LFO phenomenon in the railway traction network is not easy. Alternatively, the railway traction network can be emulated using a power electronic converter, which would feed the train power converter under test. This paper addresses the design of a network emulator able to reproduce the dynamic behavior of the actual network at low frequencies, including LFO. Three different options will be considered for the network emulator. Their performance will be studied first by means of simulations. Finally, the selected solution will be verified on a downscale test bench.

INDEX TERMS Low-frequency oscillations, resonant stability, railway system, traction unit, railway traction power supply, catenary emulator, power-hardware-in-the-loop, real-time simulation, grid-forming voltage source inverter.

I. INTRODUCTION

Modern onboard railway systems include a large number of power electronic converters aimed to improve the controllability and efficiency of the train. While the benefits brought by power electronic converters are undoubtful, dynamic interactions among these and the railway traction network can produce undesired phenomena which might result in power system instability, including low-frequency oscillations (LFO) [1], [2], [3], [4], [5], [6], [7].

LFO have been reported worldwide for different types of railway traction networks under different operating conditions, see Table 1. This phenomenon leads to a large variation of the catenary voltage and current at relatively low frequencies, typically in the range of 10%-30% the fundamental frequency (f_0) [4]. Harmful consequences of

TABLE 1. Reported LFO cases.

N °	Case	f_0 (Hz)	f_{osc} (Hz)	Year
1	Zürich, Switzerland [1]	16.7	5	1995
2	Norway [2], [3]	16.7	1.6	2007
3	Washington, USA [4]	25	3	2006
4	Siemens test, Germany [5]	50	7	2006
5	Thionville, France [6]	50	5	2008
6	Hudong Depot, China [7]	50	2-4	2008
7	Shanhaiguan Hub, China [7]	50	6-7	2011

The associate editor coordinating the review of this manuscript and approving it for publication was Sze Sing Lee.

such events include malfunction of protection systems, overvoltages/overcurrents that could damage the electrical/electronic equipment, transportation delays, among others [5], [7].

Different methods such as pole migration analysis [4], [8], [9] and impedance-based analysis [6], [10], [11], [12] have been used to study the LFO phenomenon. In these methods, the network impedance and the train input admittance are required to determine the railway system stability. The network impedance should be provided by the grid infrastructure administrator. On the other hand, the train input admittance can be measured using a frequency response test [6]. Alternatively, the train admittance can be obtained from analytical models [7], [13]. However, these models have been reported not to be accurate enough [14].

In [2], [5], it was concluded that LFO are influenced by the negative train input admittance, which appears due to the train behaving as a constant power load. On the contrary, regenerative breaking will inject power into the grid, improving stability [2]. So, LFO will only appear in motoring operation mode.

The LFO phenomenon has been mainly reported both for multiple trains in depot [6], [7] and for a train operating at a very long distance from the substation [2], [5]. This paper focuses on this last scenario. Therefore, the stability limit of the railway system for LFO will be defined as the maximum distance that a traction unit (i.e., a train) consuming a certain amount of power can reach from the substation. The maximum distance is associated with a maximum value of the network impedance. This limit is influenced by the train parameters such as transformer leakage inductance, DC-link capacitance, voltage and current control design and bandwidths, and the synchronization method used by the onboard catenary-side converter [11].

Testing the LFO phenomenon in a railway traction network is not easy, as the results would only be valid for that specific network, also it could affect other users operating in the catenary line [1]. Alternatively, train-network interactions can be studied by means of simulations. Available approaches for this purpose would include off-line simulations; real-time simulation platforms such as software-in-the-loop (SIL); hardware-in-the-loop (HIL); and power-hardware-in-the-loop (PHIL), each having advantages and disadvantages. Off-line simulations are commonly used during the initial analysis. However, real-time simulations are required at further development stages to properly evaluate the performance of the control. Only real-time options are considered in this paper.

SIL simulation integrates the compiled source control code into a time simulation. In HIL solutions, the source code is implemented on the actual control platform; different options exist in this case, mainly related to time resolution, e.g., depending on whether switching events are reproduced or only the average behavior over a switching period is considered. Independently of the implementation being used, no physical power flow occurs.

Finally, PHIL usually is made up of two parts: the emulator, and the unit under test (UUT). The emulator consists of an electronic power converter and associated real-time control, which interacts with the UUT, involving power exchange [15], [16]. This allows testing of UUT parts such as power semiconductor devices, transformers, capacitors, and inductors under close-to-real-world operating conditions before their integration in the real system.

The aim of this paper is to design, model, and build an emulator prototype of the railway traction network, able to reproduce the low-frequency oscillation phenomenon. In this study, the UUT consists of a four-quadrant power converter (4QC), which is responsible for generating the DC-link feeding all onboard systems. The interactions between the emulator and the 4QC should reliably reproduce the LFO phenomenon occurring in the real railway traction system. The emulator will be used to validate the response of the 4QC in adverse scenarios regarding LFO, and redesign train voltage and current controllers if needed. Furthermore, control mitigation techniques implemented in the controllers of traction units such as in [3] could be tested in this platform.

The paper is organized as follows: section II describes the railway system model further used for the LFO study; section III deals with LFO description and modelling; section IV discusses different design options for the emulator; section V presents the filter design for the train-emulator connection; simulation results are presented in section VI; section VII deals with the test bench construction and experimental results; finally, conclusions are drawn in section VIII.

It is finally noted that the prototype shown in this paper is intended as a proof of concept and was designed for downscale power and voltage values (10 kW AC 200 V/50 Hz), which are significantly smaller than the actual (full-rated) system values (n-hundred kW AC 25 kV/50 Hz). Based on this experience, the design of a full-rated emulator with the concepts proposed here is ongoing.

II. RAILWAY SYSTEM MODEL

A simplified representation of the railway system is shown in Fig. 1. It consists of two main elements: the traction network (i.e., power supply network) and the train [10], [12], [17], [18]. The power supply network is composed of an ideal voltage source which can be DC or AC, and the transmission line (i.e., catenary line). AC 25 kV/50 Hz electric power supply is considered here. For the study of LFO, an equivalent circuit of the transmission line based only on resistance and inductance is widely used [1], [5], [7], [9], as line capacitive effects can be safely neglected at low frequency. Fig. 2 shows the equivalent railway system model that will be used in this study, where v_c is the catenary voltage at PCC between the network and the train, and i_s is the catenary current. Network inductance (L_s) and resistance (R_s) vary almost linearly with the catenary line length (i.e., the distance between the substation and the train).

The main elements in the train are: power transformer, L-filter, single-phase four-quadrant power converter (4QC),

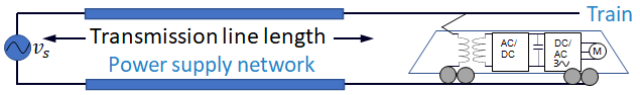

FIGURE 1. Simplified representation of the railway system. AC 25 kV/50 Hz electric power supply is considered in this work.

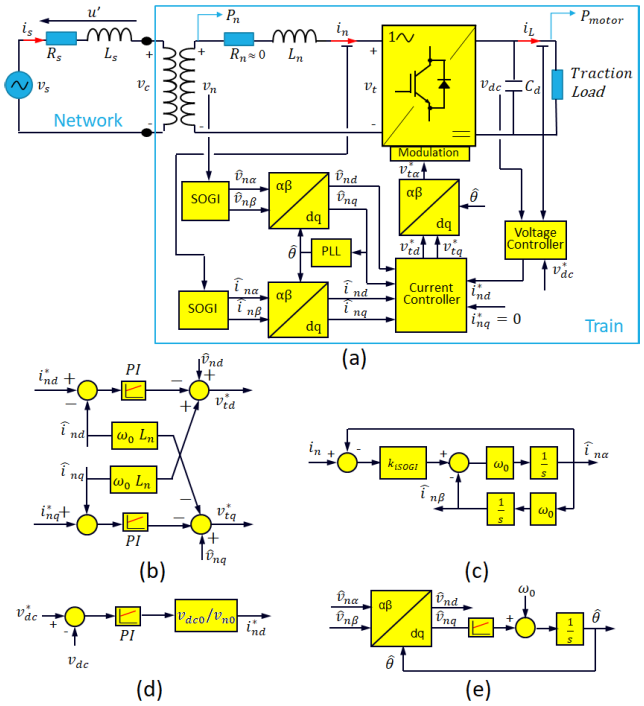

FIGURE 2. Railway control system model. (a) Train-Network model, (b) Current controller, (c) SOGI, (d) DC Voltage controller, (e) PLL.

DC-link capacitor, and traction drives consisting of inverters and motors. The 4QC behavior will determine the interaction between the train and the network [1], [5], [8], [9]. On the other hand, switching harmonics will not affect the low-frequency dynamics involved in the LFO phenomenon [8], [17]. It is safe therefore to replace the traction drives by an equivalent linear load as shown in Fig. 2, enormously simplifying analysis and simulations.

A cascaded control structure consisting of an outer voltage control loop and an inner current control loop is used. Therefore, the DC-link voltage v_{dc} is regulated through the controlled train current i_n. The 4QC control shown in Fig. 2 operates in dq coordinates, aligning the d-axis with the catenary voltage complex vector. Current and voltage controllers were tuned using zero-pole cancellation as described in [19], with BW_{CC-t} and BW_{VC-t} being the corresponding bandwidths (subscript $_t$ stands for train control parameters, to distinguish from emulator parameters, $_e$, discussed later). A phase-lock loop (PLL) is used to obtain the estimated grid voltage phase angle $\hat{\theta}$, which is required for the coordinate transformations into the synchronous reference frame [13]. The PLL was designed and tuned as described in [20], where the selection of the proportional gain k_{i-PLL} involves a trade-off between PLL filtering capability and dynamic response, and the integral gain is chosen as $k_{i-PLL} = k_{p-PLL}^2/2$. A second-order generalized integrator (SOGI) is used to obtain the quadrature signals. The gain k_{i-SOGI} of the second order generalized integrator (SOGI) was chosen as described in [5].

III. LFO MODELING

An example of the catenary line voltage and train current waveforms when the LFO phenomenon occurs, and the corresponding harmonic spectra, are shown in Fig. 3 [9]. The fundamental frequency of the AC signals is f_0, with their magnitude (envelope) varying at a frequency f_{osc}. The frequency spectra show the fundamental component f_0 with two sideband components at $f_L = f_0 - f_{osc}$ and $f_H = f_0 + f_{osc}$ respectively. The fundamental angular frequency is defined as $\omega_0 = 2\pi f_0$.

The waveforms in Fig. 3 can be approached as (1).

$$\begin{aligned} u(t) &= U(t)\sin(2\pi f_0 t) \\ &= [U_0 + \Delta U\cos(2\pi f_{osc} t)]\sin(2\pi f_0 t) \end{aligned}$$

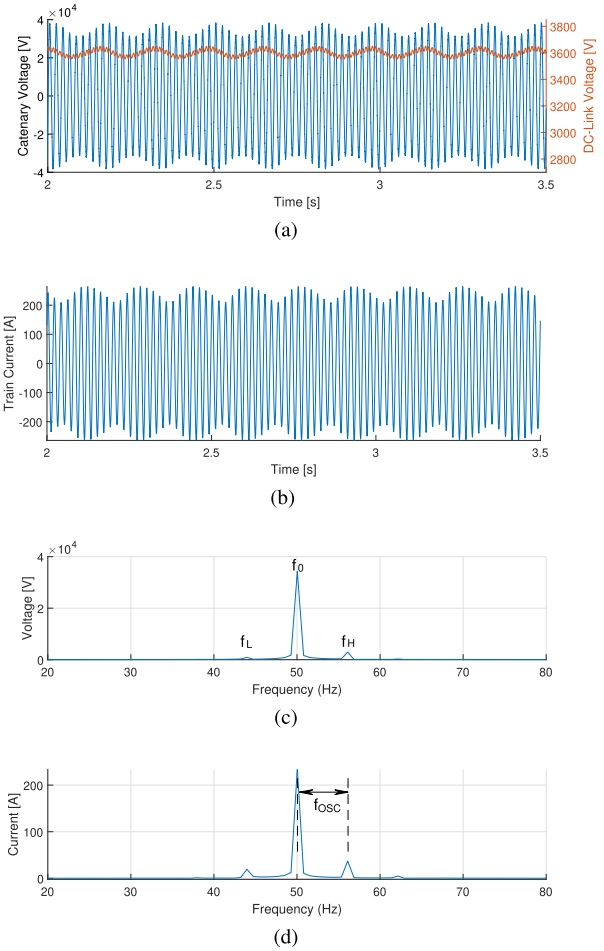

FIGURE 3. Simulation results. AC 25 kV/50 Hz railway power supply. (a) Catenary line voltage and train DC-Link voltage. (b) Train current. Frequency spectrum of (c) catenary line voltage and (d) train current FFT.

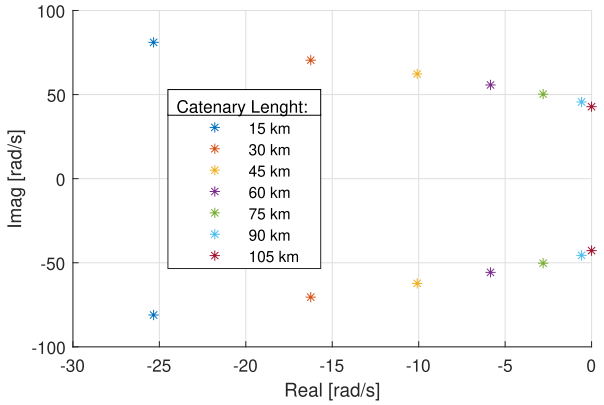

FIGURE 4. Eigenvalue migration for different catenary line length.

$$= U_0 \sin(2\pi f_0 t) + \frac{\Delta U}{2} \sin(2\pi f_L t) + \frac{\Delta U}{2} \sin(2\pi f_H t) \quad (1)$$

A widely used approach for LFO analysis is to develop a small signal model of the power network and train input admittance [8]. Fig. 4 shows an example of the dominant eigenvalue migration of the resulting system as the catenary line length increases [9]. The stability limit occurs when the eigenvalues cross the imaginary axis of the complex plane [8]. It is observed that the risk of instability increases with the distance from the substation. The frequency at which the eigenvalues cross the imaginary axis corresponds to f_{osc} in (1).

IV. TRACTION NETWORK EMULATOR DESIGN

This section discusses different approaches for the design of the railway traction network emulator aimed to reproduce the LFO phenomenon. In order to perform this task, the emulator should be able to simulate the railway system dynamics for changing values of the network resistance (R_s) and the network inductance (L_s) with the variable distance from the train to the substation.

A. SYSTEM DESCRIPTION

As discussed in Section II, the two main elements of the railway system model are the power supply network (i.e., ideal voltage source and varying impedance) and the train (see Fig. 5a). The power supply emulator replaces the power supply network feeding the train as shown in Fig. 5b and Fig. 5c. The emulator consists of two main structures:

- Real-time simulator. It reproduces the dynamic behavior of the power supply network in real-time, its output being the catenary voltage reference, v_c^*. Its design is discussed in Subsection IV-B.
- Single-phase voltage source inverter (VSI) operating in a grid-forming mode. It supplies the desired catenary voltage v_c to the train, it is described in Subsection IV-C.

It is noted that in the railway system model from Fig. 2, the power supply network current i_s and the train current i_n are different due to the step-down transformer present in the traction unit. For the analysis in this section, the transformer will not be considered, therefore $i_s = i_n$ as shown in Fig. 5a. However, it was preferred to keep both current definitions in the schematics to visualize the actual physics of the system.

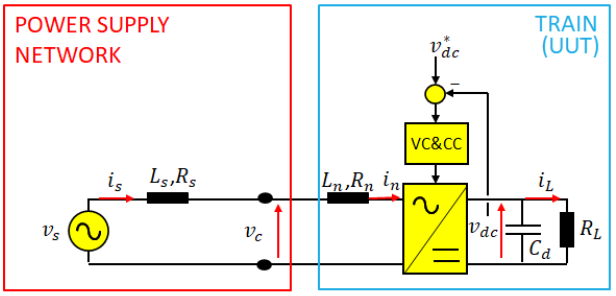

(a) Railway system model

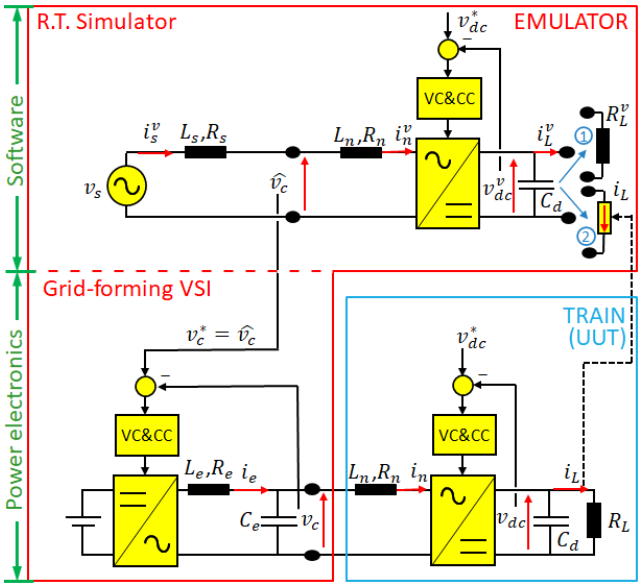

(b) Emulator model: Options 1 (Open loop) - Resistive load
Option 2 (Closed loop) - Controlled current source

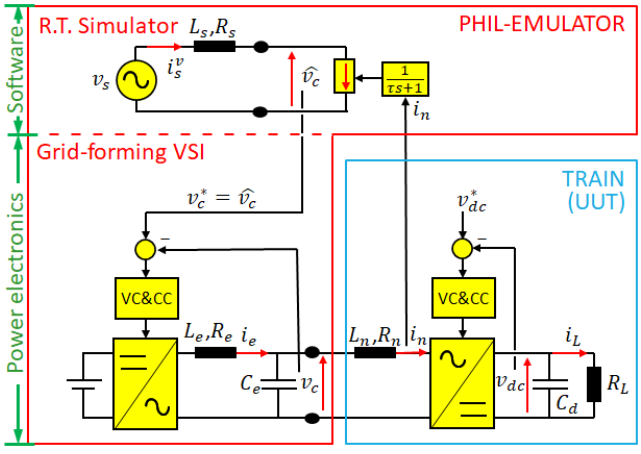

(c) PHIL-Emulator model (Option 3)

FIGURE 5. Railway system model and emulator models. Superscript "v" indicates virtual variables.

B. REAL-TIME SIMULATOR

The design of the real-time simulator is not trivial. Three different options will be discussed, which correspond to different stages of this research, i.e., later options improve the limitations found in the preceding ones. The reason to include earlier designs is to highlight those aspects which will play a relevant role in accurate emulation of the LFO phenomenon occurring in the railway system.

For the discussion following, variables that exist only in the simulator, i.e., virtual variables, will be indicated by a superscript "^{v}". There are variables that coincide both in the virtual domain and in the physical domain. Such variables are labeled without "^{v}" superscript.

1) OPTION 1: OPEN-LOOP

In this option, the simulator generates the catenary voltage reference, v_c^*, simulating the complete railway system. The configuration is shown in Fig. 5b. The simulator includes a virtual power supply network and a virtual train. The load connected to the virtual DC-link is a constant resistance R_L^v. This option requires previous knowledge of train parameters as it runs in parallel with the physical train (i.e., real train). Furthermore, there is no feedback from the physical train to the emulator. Consequently, this option works only properly for constant values of train load R_L, since in this case, $R_L^v = R_L$. However, if a change in load R_L is desired, it should simultaneously occur along with a change in R_L^v in the virtual domain, which can be problematic due to the lack of information that the emulator receives from the physical train. Option 2 overcomes this drawback, as will be discussed following.

2) OPTION 2: CLOSED-LOOP

This option is also shown in Fig. 5b. R_L^v is now replaced by a controlled current source as a virtual load. By doing this, the load current in the simulator will track the measured load current i_L which circulates through the real load R_L. Therefore, this option allows emulation with varying loads.

Regardless of this improvement, a drawback of both options 1 and 2 is they require in advance precise knowledge of control design and tuning of the UUT to emulate catenary voltage dynamics, which is not often available. The approach discussed next is aimed at overcoming this drawback.

3) OPTION 3: PHIL

This option is shown in Fig. 5c. A virtual RL circuit is used to obtain the estimated catenary voltage $\widehat{V}_c(s)$. From the railway system model in Fig. 5a, the equation defining the catenary voltage $V_c(s)$ is given by (2).

$$V_c(s) = V_s(s) - (L_s s + R_s)\, I_s(s) \tag{2}$$

Since this equation is a non-causal system, it cannot be used for estimation purposes. A low-pass filter is then added for real-time implementation, see (3) and Fig. 6. A time constant of $\tau = 31.8\ \mu$s was selected, corresponding to a cut-off frequency of 5 kHz. This is the maximum frequency complying with the Nyquist-Shannon criteria considering 10 kHz as the sampling frequency of the grid-forming VSI [21].

$$\widehat{V}_c(s) = V_s(s) - \frac{(L_s s + R_s)}{\tau s + 1} I_n(s) \tag{3}$$

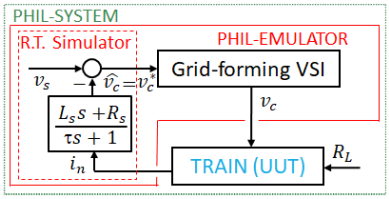

FIGURE 6. Real-time simulator block diagram in the PHIL system.

A simplified representation of a PHIL system is shown in Fig. 6. Here, the closed-loop configuration that the real-time simulator creates between the grid-forming VSI and the train is easily seen. An appealing characteristic of this option is that it does not require previous knowledge of train characteristics. The train can be considered a black box, the emulator behaving as a power supply network whose properties are independent of the load (i.e., train). This option also allows the implementation and testing of controls strategies aimed to mitigate LFO such as Power-Oscillation-Damping [3] and Virtual-Impedance-Based Suppression Method [22].

C. GRID-FORMING VSI

The block diagram of the single-phase VSI is shown in Fig. 7. It consists of a two-level single-phase converter (H-bridge), which is fed from a voltage source on the DC-side, and has an LC filter connected to its AC side. Unipolar modulation is used in this study.

A cascaded control is used as shown in Fig. 7. The inner loop controls the inductor current i_e, while the outer loop controls the capacitor voltage v_c (i.e., catenary voltage), to which the traction unit is connected.

Current control is performed in a stationary reference frame using a proportional-resonant (PR) controller as shown in Fig. 7(b). The corresponding transfer function is given by (4), where k_{p-cc} and k_{r-cc} are the gains to be tuned to obtain the desired closed loop current control bandwidth BW_{CC-e} [23], see (5) and (6). The basic concept of the PR controller is to obtain an infinite gain at a selected resonant frequency, as this will guarantee zero steady-state error at that frequency. The resonant controller can be seen therefore as a generalization of the PI controller, in which the infinite gain occurs not at DC, but at the desired frequency. The resonance frequency is the fundamental frequency f_0. The coefficient K_f adjusts the bandpass in (4), it takes values from 0.25 to 1 [23]. Furthermore, in Fig. 7(b) the measured train

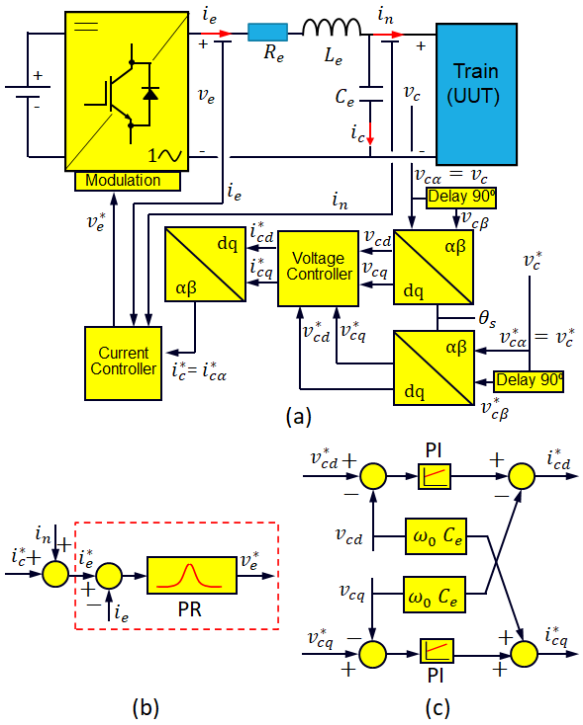

FIGURE 7. Grid-forming single-phase VSI. (a) Overall block diagram, (b) Current controller, (c) Voltage controller.

current i_n is added to the current command as a feed-forward term to improve the dynamic response of the voltage control loop [19].

$$PR(s) = 2k_{p-cc}\frac{s^2 + s\left(k_{r-cc}/k_{p-cc}\right) + (2\pi f_0)^2}{s^2 + (2\pi f_0)^2} \tag{4}$$

$$k_{p-cc} = \sqrt{2}\,(2\pi BW_{CC-e})\,L_e \tag{5}$$

$$k_{r-cc} = K_f\,(2\pi BW_{CC-e})^2\,L_e \tag{6}$$

The catenary voltage control is performed in a synchronous reference frame using a PI controller as shown in Fig. 7c, where the proportional gain and the integral gain are given by (7) and (8) as function of the desired voltage control bandwidth BW_{VC-e}.

$$k_{p-vc} = \sqrt{2}\,(2\pi BW_{VC-e})\,C_e \tag{7}$$

$$k_{i-vc} = (2\pi BW_{VC-e})^2\,C_e \tag{8}$$

A virtual quadrature component of the catenary voltage is obtained by delaying 90 degrees the alpha component. For that purpose, the filter in (9) is used. Feedforward terms are used in the voltage controller to eliminate cross-coupling between $d-$ and $q-$axes, see Fig. 7c.

$$G_{Delay-90}(s) = \frac{2\pi f_0 - s}{s + 2\pi f_0} \tag{9}$$

D. MULTIPLE TRAINS

From Subsections IV-C to IV-A, it is noted that the emulator is aimed to replace the traction network. For the case when multiple trains are in the depot (i.e., located at the same place), it does not modify the network topology since all the trains are connected in parallel. Therefore, only one train with an equivalent input admittance can be used.

On the other hand, for the case of multiple trains operating in the same power supply section at different locations, the network topology must be modified to include additional connection nodes, therefore, the virtual network in the real-time simulator must be modified, but the proposed methodology would still apply. Also, additional virtual trains can be added.

These analyses are not included in this article due to space constraints, but it is worth it to mention them.

V. INVERTERS AND FILTER DESIGN

Design of inverters and passive elements of the downscale prototype is addressed in this section. A similar methodology would be followed for the full-rated emulator.

As observed from Fig. 5b, grid-forming VSI and 4QC are connected through $LC + L$ filters. L_n corresponds to the inductance seen by the 4QC (see Fig. 2). It should be large enough to filter the current harmonics, but realizing that excessively large values will limit power transfer capability. Therefore, a trade-off is required. For simulations and test bench, a DC-link voltage $V_{dc} = 300$ V has been selected for the inverters, with a catenary peak voltage of $V_c = 200$ V. These voltages were chosen to provide a large safety margin with respect to power devices and DC-link capacitor voltage limits, as some of the experiments reproducing LFO might produce large excursions of the voltages. Nominal power of 10 kW, with a current ripple $< 4\%$ of the train nominal current have been defined as design targets.

The maximum transfer power with a unity power factor between train and network is given by (10) [24]. From this equation, a value of $L_n = 7.1$ mH is obtained to transfer the targeted power $P_n = 10$ kW. Due to availability issues, a value of $L_n = 6$ mH was selected.

$$P_n = \frac{\sqrt{V_c^2 V_{dc}^2 - V_c^4}}{2X_n} \tag{10}$$

Current ripple can be approached using (11), where load angle ψ is the phase difference between catenary voltage v_c and the 4QC terminal voltage v_t [24].

$$\Delta i(\%) = \frac{\pi\sqrt{(2)}V_c\,(1 - (V_t/V_{dc})\cos(\psi))}{(f_{sw}/f_0)X_n I_n}100 \tag{11}$$

For the targeted current ripple limit of 4 % and the selected value of L_n, the switching frequency provided by (11) is $f_{sw} = 7.5$ kHz. A slightly larger value, $f_{sw} = 10$ kHz, was finally chosen.

Once L_n is selected, there would be two degrees of freedom for the design of catenary emulator LC filter [25]. An option in this case is to analyze the $LC + L$ filters as an equivalent LCL filter. It is advantageous for the design of LCL filters to have the same values for both inductances, as this minimizes the size of the filter components [26].

Assumed that the inductances have been selected such that $L_e = L_n = L$, and neglecting the resistive terms of

inductances and capacitors, the transfer function between the capacitor voltage at the point of coupling (i.e., v_c) and the voltage being applied by any of the two inverters (i.e., v_t,v_e) is given by (12). The filter behaves as a second order system, an undamped resonance occurring at the cut-off frequency ω_c which is given by (13).

$$\frac{V_c(s)}{V(s)} = \frac{1}{s^2 LC_e + 2} \tag{12}$$

$$\omega_c = \sqrt{\frac{2}{LC_e}} \tag{13}$$

Capacitor C_e was chosen to get a cut-off frequency around 600 Hz, which is much higher than the fundamental frequency but far enough from the switching frequency. The parameters of 4QC and VSI filters are presented in Tables 2 and 3 respectively. Fig. 8 shows the resulting Bode diagram from (12). It is observed that the attenuation at the switching frequency is larger than −50 dB.

TABLE 2. Train-network parameters.

Symbol	Description	Value
Power supply network		
L_s	Line Inductance (Limit)	10 mH
R_s	Line Resistance (Limit)	150 mΩ
V_s	Supply Voltage Amplitude	200 V
f_0	Fundamental Frequency	50 Hz
Train (4QC)		
L_n	4QC Inductance	6 mH
R_n	4QC Resistance	10 mΩ
f_{sw}	Switching Frequency	10 kHz
BW_{VC-t}	Voltage Control Bandwidth	10 Hz
BW_{CC-t}	Current Control Bandwidth	100 Hz
R_L	Resistive Load	200 Ω
V_{dc}	DC-link Voltage	300 V

Any topology able to produce a single-phase AC voltage with a fundamental frequency of 50 Hz would be suitable for grid-forming VSI. Two issues should be considered. First, since the LFO will occur when the active power is flowing from emulator to 4QC, the grid-forming converter will not

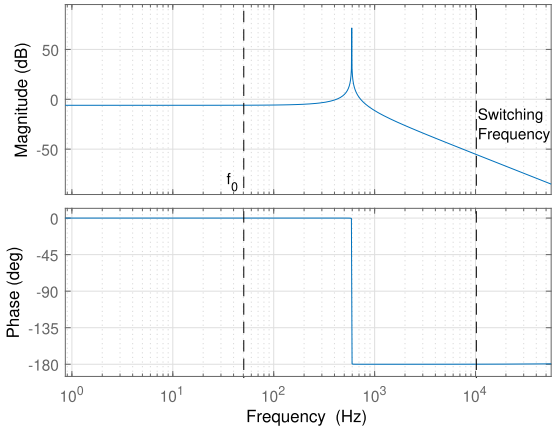

FIGURE 8. Bode diagram of capacitor vs. inverter voltage. $V_c(j\omega)/V(j\omega)$.

TABLE 3. Network emulator parameters.

Symbol	Description	Value
L_e	Emulator Inductance	6 mH
R_e	Emulator Resistance	10 mΩ
C_e	Emulator Capacitance	24 mF
f_{sw}	Switching Frequency	10 kHz
BW_{VC-e}	Voltage Control Bandwidth	50 Hz / 100 Hz
BW_{CC-e}	Current Control Bandwidth	500 Hz / 1000 Hz

be required to absorb power. Second, to reduce the effects of switching harmonics produced by the grid-forming inverter and ease the design of the LC filter at the output of the emulator, high switching frequencies and/or multilevel topologies (e.g., NPC) are preferable, however, cost and control complexity must be also considered. A two-level full bridge has been used for the downscale prototype developed in this paper. The same topology has been considered for the 4QC.

VI. SIMULATION RESULTS

In this section, time domain simulations of the emulation methods proposed in Section IV (see Fig. 5) are carried out to test their performance.

The behavior of the railway system model in Fig. 5a will be first simulated in Subsection VI-A to be later used as a reference to assess the performance of the different methods. Power supply network parameters and train control parameters are shown in Table 2.

Regarding the catenary emulator, it has been observed during this work that the bandwidths of the voltage and current controllers of the grid-forming VSI will strongly affect to the emulator capability to accurately reproduce LFO. To illustrate this, the behavior of the different emulator designs was tested for two different sets of control bandwidths; set #1 is ($BW_{VC-e} = 50$ Hz, $BW_{CC-e} = 500$ Hz), and set #2 is ($BW_{VC-e} = 100$ Hz, $BW_{CC-e} = 1000$ Hz). Emulator parameters are shown in Table 3. On the other hand, train voltage and current control bandwidths, BW_{VC-t} and BW_{CC-t}, were kept constants for all the cases.

A. LFO USING RAILWAY SYSTEM MODEL

Fig. 9 shows the DC-link voltage, catenary voltage, and train current using the railway system model shown in Fig. 5a, when step-like changes in network impedance occur. Such changes would reproduce the effect of increasing the transmission line length from the substation transformer to the traction unit. It is noted that while step-like changes will not occur in the real system, still they are a useful excitation to obtain the damping ratio, settling time, oscillation frequency, and eigenvalues for the system time response. Indeed, step-like changes they have been frequently used for LFO and stability studies [1], [5], [8]. It is observed from Fig. 9 that LFO progressively develop when the impedance increases keeping constant the L/R ratio, the stability limit occurring at $L_s = 10$ mH and $R_s = 150$ mΩ.

Since increasing the network impedance decreases system damping and increases the settling time, it is inferred that

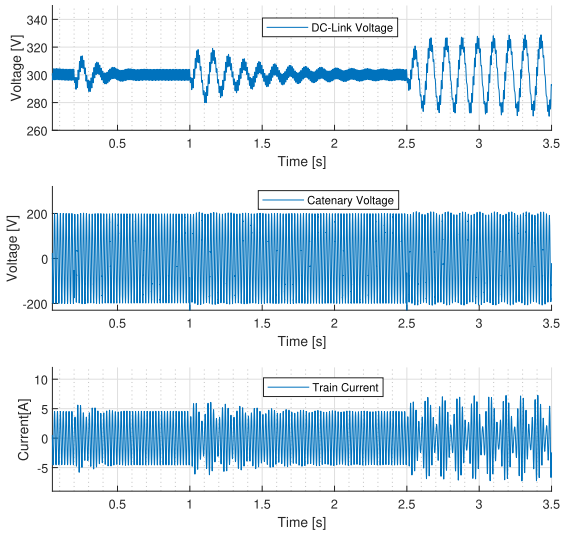

FIGURE 9. Simulation results. LFO when line inductance and resistance increase from ($L_S = 4$ mH, $R_S = 60$ mΩ) to ($L_S = 10$ mH and $R_S = 150$ mΩ) in steps of $\Delta L_S = 2$ mH and $\Delta R_S = 30$ mΩ) at t = 0.2 s, t = 1 s, and t = 2.5 s.

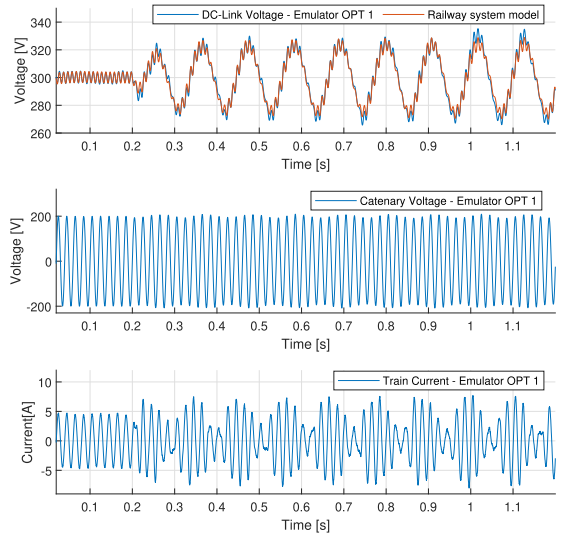

FIGURE 10. Simulation results using option 1 for emulator. Line impedance increases from $L_S = 8$ mH, $R_S = 120$ mΩ to $L_S = 10$ mH, $R_S = 150$ mΩ at $t = 0.2$ s. From top to bottom: DC-link Voltage, catenary voltage and train current. $BW_{CC-e} = 500$ Hz, $BW_{VC-e} = 50$ Hz.

critical system eigenvalues move from the negative real side of the complex plane (i.e., stable region) to the right (i.e., unstable region). At the stability limit, the real component of critical eigenvalues is zero, and the imaginary component can be identified from the oscillation frequency, which is $f_{osc} \approx 9$ Hz.

B. LFO USING OPEN-LOOP EMULATOR (OPTION 1)

Fig. 10 shows LFO when network inductance and resistance increase using option 1 of the emulator in Fig. 5b. Only the results for set #1 of voltage and current control bandwidths are presented, as no significant differences were found for this particular case when using set #2.

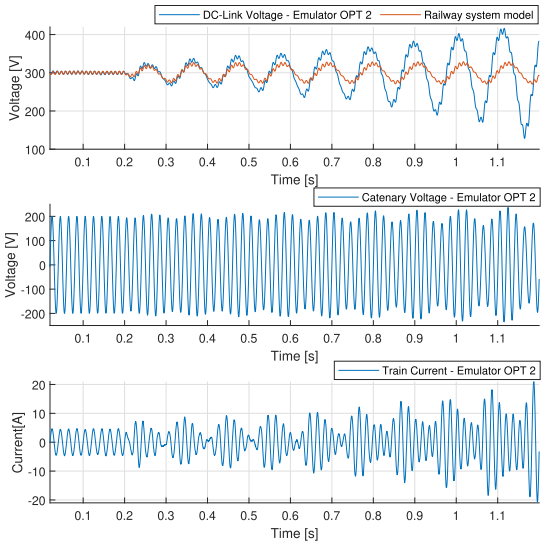

(a) $BW_{VC-e} = 50$ Hz, $BW_{CC-e} = 500$ Hz

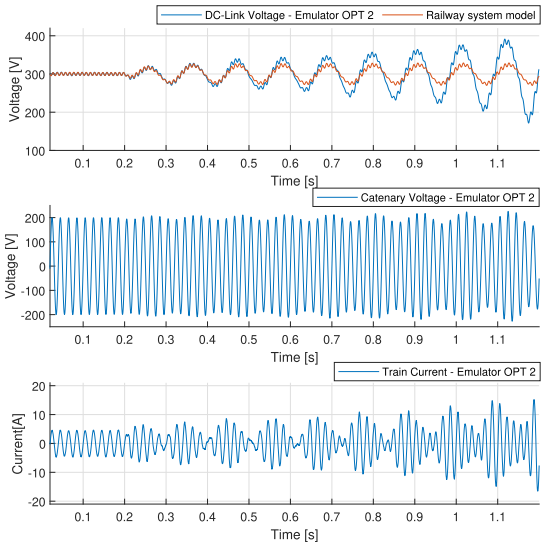

(b) $BW_{VC-e} = 100$ Hz, $BW_{CC-e} = 1000$ Hz

FIGURE 11. Simulation results using option 2 for the emulator. Line impedance increases from $L_S = 8$ mH, $R_S = 120$ mΩ to $L_S = 10$ mH, $R_S = 150$ mΩ at $t = 0.2$ s. From top to bottom: DC-link Voltage, catenary voltage and train current.

The DC-link voltage response of the real railway system model is also shown in Fig. 10 for comparison purposes. A good agreement is observed between real and emulated systems. However, simulations using this option are only possible if the load R_L is constant, and the precise knowledge of train control design is available as discussed in Subsection VI-F, which might not be always possible.

C. LFO USING CLOSED-LOOP EMULATOR (OPTION 2)

Time-domain simulation results using the emulator model option 2 are shown in Fig. 11 for the two different sets of controllers bandwidths. As shown in Fig. 11a, the system

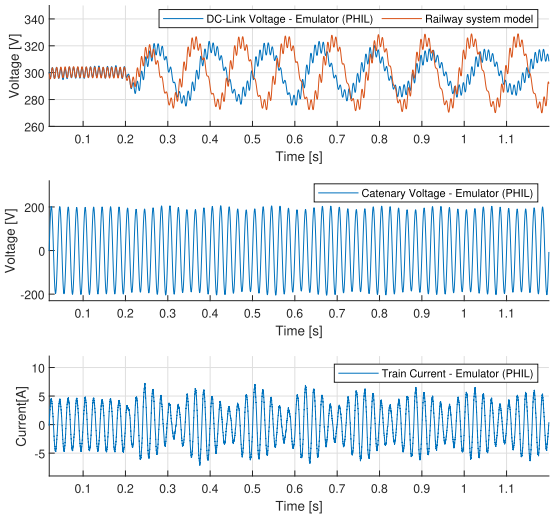

(a) $BW_{VC-e} = 50$ Hz, $BW_{CC-e} = 500$ Hz

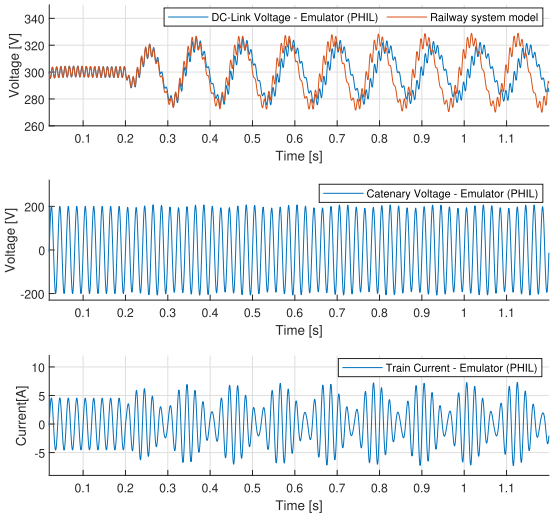

(b) $BW_{VC-e} = 100$ Hz, $BW_{CC-e} = 1000$ Hz

FIGURE 12. Simulation results using option 3 for the emulator. Line impedance increases from $L_S = 8$ mH, $R_S = 120$ mΩ to $L_S = 10$ mH, $R_S = 150$ mΩ at $t = 0.2$ s. From top to bottom: DC-link Voltage, catenary voltage and train current.

becomes unstable when the change in line impedance is applied. Increasing VSI control bandwidth slightly reduces the rate of increase of the oscillations, but still, the system is unstable as shown in Fig. 11b. These results suggest that the use of this option is not advisable as it fails to reproduce the LFO phenomenon.

D. LFO USING PHIL EMULATOR (OPTION 3)

Time domain simulations using the PHIL-Emulator are shown in Fig. 12. The case for bandwidths set #1 is shown in Fig. 12a. The response is seen to be more damped compared to the actual power system response, LFO also occurring at

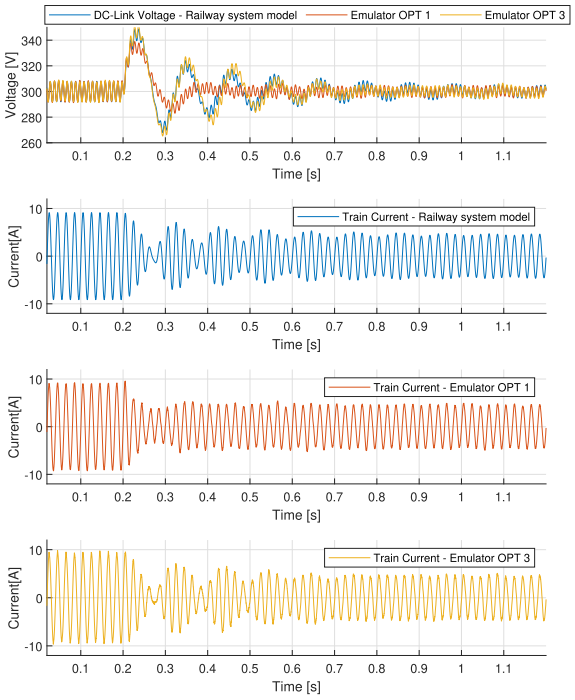

FIGURE 13. Simulation results using network emulator options 1 and 3. Line impedance $L_S = 8$ mH, $R_S = 120$ mΩ. Load step change from $R_L = 100$ mΩ to $R_L = 200$ mΩ at $t = 0.2$ s. Control bandwidths: $BW_{CC-e} = 1000$ Hz, $BW_{VC-e} = 100$ Hz.

lower frequencies (8 Hz for emulator vs. 9 Hz for the actual railway system model). The improvement when VSI controllers bandwidths are increased can be observed in Fig. 12b, but oscillations are seen still to be slightly damped and occur at a slightly lower frequency compared to the actual railway system case.

E. RESPONSE TO LOAD CHANGES (VARIABLE R_L)

Time domain simulations showing the response to step change in the load using the emulator model options 1 and 3 are shown in Fig. 13. Option 2 was not considered for this test since its performance has already been found to be inferior in Subsection VI-C.

From Fig. 13 the emulated systems and the railway system reach the same steady-state, however, they present different dynamics, this can be appreciated in the transient state. The emulator option 1 is not capable to emulate the railway system dynamic for this type of test, on the other hand, option 3 is able to reproduce the phenomenon accurately.

F. SUMMARY

It is concluded from the simulations presented in this section that the highest accuracy in reproducing LFO would be obtained using Option 1 for the emulator. However, this option implies that current and voltage control structures and tuning are the same for emulator and actual train, which might be difficult to achieve or even impossible in practice. It is interesting to note although the simulation for this option was performed in real-time, this is not actually required,

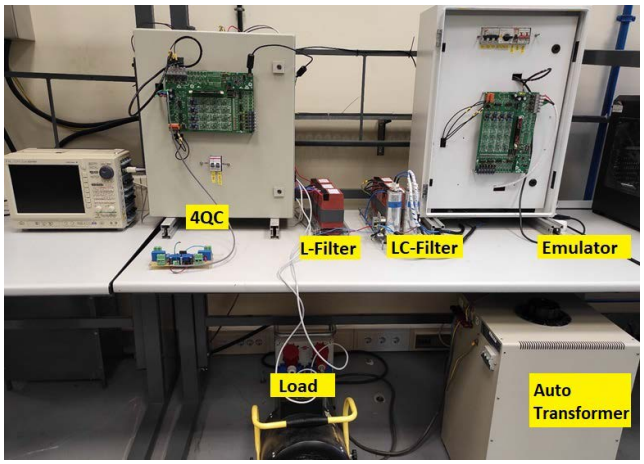

FIGURE 14. Experimental test bench.

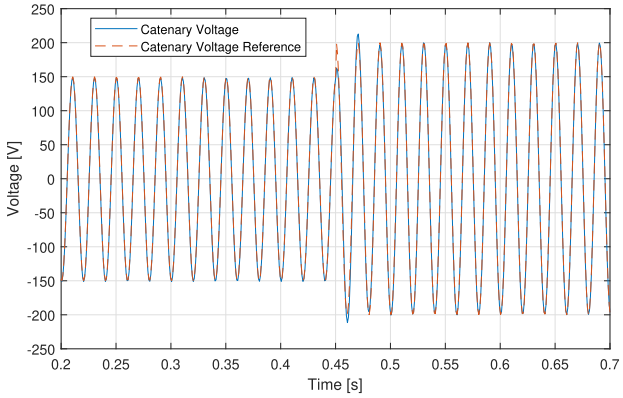

FIGURE 15. Experimental results. Catenary voltage step response. From $V_c = 150$ V to $V_c = 200$ V at t = 0.45 s.

as there is no feedback from the real train to the emulator. Therefore, it would be perfectly possible to simulate the train behavior off-line and use the catenary voltage resulting from the simulation to provide the reference signal to emulator v_c^* (see Fig. 5b).

In contrast with option 1, option 2 includes a feedback mechanism as it uses the train load current i_L to feed the emulator. However, this method still requires knowledge of train controllers. Furthermore, it is observed from simulation results that this option has the worst accuracy in reproducing the behavior of the actual power system.

Finally, option 3 shows good accuracy in reproducing LFO, and doesn't require knowledge of train control, making it especially appealing.

G. DISCUSSION

As already explained, the low-frequency oscillations are produced by the dynamic interaction between the power supply network and the train (i.e., 4QC) [13]. For option 1 of the emulation; the dynamic interaction which provokes LFO, happens entirely in the simulator between the virtual power

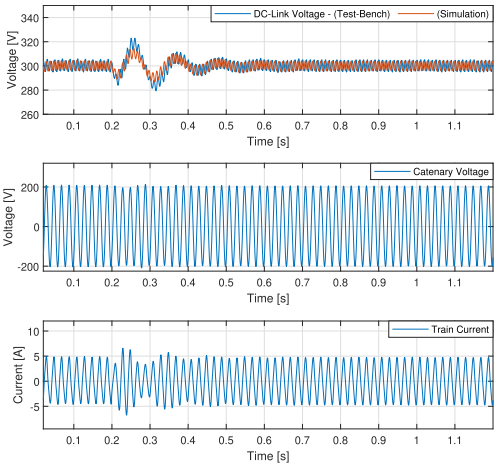

(a) $L_s = 4 \rightarrow 6$ mH, $R_s = 60 \rightarrow 90$ mΩ

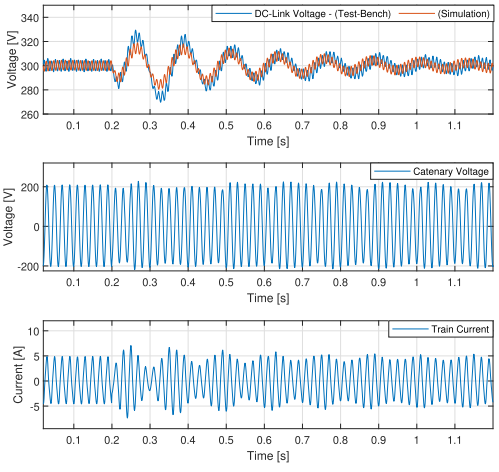

(b) $L_s = 6 \rightarrow 8$ mH, $R_s = 90 \rightarrow 120$ mΩ

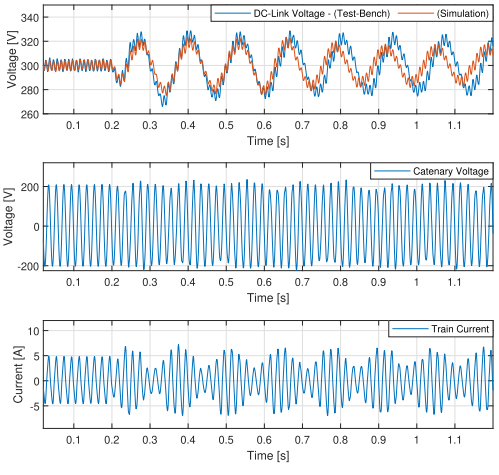

(c) $L_s = 8 \rightarrow 10$ mH, $R_s = 120 \rightarrow 150$ mΩ

FIGURE 16. Experimental results. System response to step-like changes in power network impedance as indicated in the captions. Changes occur at t = 0.2 s. For each case, from top to bottom: DC-link voltage, catenary voltage, and train current. Simulation results are shown for comparison.

supply and the virtual train. In this option, the physical train doesn't contribute to LFO formation due to the open-loop configuration.

For option 2, the dynamic of the physical train is now in the closed-loop, and it participates in the LFO formation. This implies repeated elements in the loop. For instance, the dynamics of the 4QC voltage and current controllers affect the system twice (due to the physical train and the virtual train). Although these repeated elements do not affect the steady-state response, they add delays, which impact the transient response and the system dynamics. System delays were already reported to influence LFO instability [11], and would explain the inaccuracy of this option to reproduce the LFO phenomenon.

Using the third option (PHIL-Emulator), LFO are the result of the interaction between the virtual power supply network and the physical train. Although the dynamic of grid-forming VSI is in between, large values of voltage and current control bandwidths, which make this system fast enough, allow accurately replicating of the LFO phenomenon.

In conclusion, high control bandwidths would be desirable, as this would reduce control delays which can severely affect emulator performance. The maximum bandwidth that can be achieved would be limited by Nyquist sampling theorem in the first place. A second concern for the selection of the bandwidths would be the noise mainly coming from sensors, during implementation this was found to be indeed the main limiting factor for the selection of the gains of the controllers, see Section VII. Further, it is noted that although all the preceding discussion on the tuning of the controllers has focused on the concept of *bandwidth*, other design aspects, such as natural frequency or settling time, could be used instead for the same purpose since they also contain information about system delays. The detailed impact of additional indices, e.g., damping coefficient, might also need to be considered. A thorough analysis of the influence of controller design and tuning on emulator performance is a matter of ongoing research.

Finally, in terms of implementation in the micro-controller, option 3 requires less computational effort than the other two options, in which relatively complex electronic power converters have to be simulated in real-time.

VII. EXPERIMENTAL RESULTS

This section presents experimental results obtained using the Option 3 (PHIL-Emulator) discussed in Subsection IV-B3. The other two options were disregarded for experimental verification as they were concluded to be inferior. The test bench is shown in Fig. 14. Its design was already discussed in Section V. Power supply parameters, train parameters and emulator parameters are the same as for the simulation results in Section VI (see Tables 2 and 3).

Current control and voltage control bandwidths of $BW_{VC-e} = 50$ Hz and $BW_{CC-e} = 500$ Hz, respectively, have been used in the test bench. It was discussed in Section VI-D the relevance of emulator control bandwidths for the accurate reproduction of LFO. Unfortunately, signal noise content in the real system avoided the use of the higher bandwidths. Fig. 15 shows the catenary voltage step response to test the control action of grid-forming VSI.

Fig. 16 shows the system response to changes in the virtual catenary impedance. LFO are seen to develop as the virtual network impedance increases, eventually reaching the stability limit in Fig. 16c. Oscillation frequency at the stability limit occurs at around 8 Hz, which is in good agreement with the simulation results from Fig. 12a. The limit values of power network impedance also agree with the values obtained in the simulation. This confirms the correctness of the proposed approach.

VIII. CONCLUSION

The design of a network emulator able to reproduce the dynamic behavior of a railway traction network, including LFO, has been discussed in this paper. The emulator will allow evaluating the response of the 4QC power converter in the event of LFO in a test bench, avoiding expensive or even non-viable on-track tests.

Three different options for the catenary emulator were considered: open-loop, closed-loop, and PHIL. Simulation was used for preliminary verification. It was shown that due to the lack of feedback from the train, the first option can reproduce the LFO only when the virtual and actual traction loads are equal and constant; additionally, the first two options require precise knowledge of the train controller parameters, which might not be available. PHIL option was shown to overcome these limitations.

The study also showed that the bandwidth of the voltage and current controllers of the grid-forming VSI emulator strongly affect its capability to reproduce LFO. It was concluded that, despite the low-frequency nature of LFO events being targeted, relatively high bandwidths and proper spectral separation between voltage and current control loops bandwidths are required.

The proposed methods were tested in a test bench consisting of a grid-forming inverter and the 4QC connected through an LCL filter. Experimental results were found to be in good agreement with simulation results. Due to noise, the higher control bandwidths values used in the simulation couldn't be achieved on the test bench.

It is noted finally that the work shown in this paper is a concept validation with a downscale system rated for 10 kW. The design of a full-scale test bench is ongoing.

REFERENCES

[1] S. Menth and M. Meyer, "Low frequency power oscillations in electric railway systems," *Elektrische Bahnen.*, vol. 104, no. 4, pp. 216–221, 2006.

[2] L. Buhrkall, S. Danielsen, A. Eisele, M. Bergman, and J. Galic, "Low-frequency oscillations in Scandinavian railway power supply—Part I: Basic considerations," *Elektrische Bahnen*, vol. 108, pp. 56–64, Jan. 2010.

[3] L. Buhrkall, S. Danielsen, A. Eisele, M. Bergman, and J. Galic, "Low-frequency oscillations in Scandinavian railway power supply—Part 2: Test of traction units," *Elektrische Bahnen*, vol. 108, pp. 103–111, Mar. 2010.

[4] S. Danielsen, T. Toftevaag, and O. Fosso, "Application of linear analysis in traction power system stability studies," in *Proc. 11th Int. Conf. Comput. Syst. Design Operation Railway Transit Syst.*, vol. 103, Aug. 2008, pp. 401–410.

[5] S. Danielsen, M. Molinas, T. Toftevaag, and O. Fosso, "Constant power load characteristic's influence on the low-frequency interaction between advanced electrical rail vehicle and railway traction power supply with rotary converters," *Modern Electr. Traction*, pp. 1–6, Sep. 2009.

[6] J. Suarez, P. Ladoux, N. Roux, H. Caron, and E. Guillame, "Measurement of locomotive input admittance to analyse low frequency instability on AC rail networks," in *Proc. Int. Symp. Power Electron., Electr. Drives, Autom. Motion*, Jun. 2014, pp. 790–795.

[7] H. Wang, W. Mingli, and J. Sun, "Analysis of low-frequency oscillation in electric railways based on small-signal modeling of vehicle-grid system in *dq* frame," *IEEE Trans. Power Electron.*, vol. 30, no. 9, pp. 5318–5330, Sep. 2015.

[8] S. Danielsen, "Electric traction power system stability: Low-frequency interaction between advanced rail vehicles and a rotary frequency converter," Ph.D. dissertation, NTNU Trykk, Trondheim, Norway, 2010.

[9] P. Frutos, J. M. Guerrero, I. Muniategui, I. Vicente, A. Endemano, and F. Briz, "Low-frequency oscillations analysis in AC railway networks using eigenmode identification," in *Proc. IEEE Energy Convers. Congr. Expo. (ECCE)*, Oct. 2021, pp. 1573–1579.

[10] Y. Hachicha, D. Cypers, S. Belin, M. Meli, P. Ladoux, and N. Roux, "Towards a unified low frequency Stability criterion for 15 kV / 16.7 Hz and 25 kV / 50 Hz railway power system," in *Proc. PCIM Eur. Digit., Int. Exhib. Conf. Power Electron., Intell. Motion, Renew. Energy Energy Manag.*, 2020, pp. 1–8.

[11] P. Frutos, P. Ladoux, N. Roux, I. Larrazabal, J. M. Guerrero, and F. Briz, "Low frequency stability of AC railway traction power systems: Analysis of the influence of traction unit parameters," *Electronics*, vol. 11, no. 10, p. 1593, May 2022. [Online]. Available: https://www.mdpi.com/2079-9292/11/10/1593

[12] *Railway Applications—Fixed Installations and Rolling Stock—Technical Criteria for the Coordination Between Power Supply and Rolling Stock to Achieve Interoperability—Part 2: Stability and Harmonics*, document EN 50388-2:2017, 2017.

[13] H. Hu, H. Tao, F. Blaabjerg, X. Wang, Z. He, and S. Gao, "Train–network interactions and stability evaluation in high-speed railways—Part I: Phenomena and modeling," *IEEE Trans. Power Electron.*, vol. 33, no. 6, pp. 4627–4642, Jun. 2018.

[14] Y. Liao, Z. Liu, H. Zhang, and B. Wen, "Low-frequency stability analysis of single-phase system with *dq*-frame impedance approach—Part I: Impedance modeling and verification," *IEEE Trans. Ind. Appl.*, vol. 54, no. 5, pp. 4999–5011, Sep. 2018.

[15] Y. Huo, G. Gruosso, and L. Piegari, "Power hardware in the loop simulator of photovoltaic plant for smart grid interation analysis," in *Proc. IEEE Int. Conf. Environ. Electr. Eng. IEEE Ind. Commercial Power Syst. Eur. (EEEIC/I CPS Eur.)*, Jun. 2017, pp. 1–5.

[16] A. Castaings, A. Bouscayrol, W. Lhomme, and R. Trigui, "Power hardware-in-the-loop simulation for testing multi-sources vehicles," in *Proc. 20th IFAC World Congr.*, Toulouse, France, Jul. 2017, vol. 50, no. 1, pp. 10971–10976. [Online]. Available: https://hal.archives-ouvertes.fr/hal-01745537

[17] Y. Hachicha, D. Cypers, M. Takuefou, S. Belin, P. Ladoux, and N. Roux, "Use of a HIL railway traction simulator for low frequency network stability studies," in *Proc. IEEE Int. Conf. Electr. Syst. Aircr., Railway, Ship Propuls. Road Vehicles Int. Transp. Electrific. Conf. (ESARS-ITEC)*, Nov. 2018, pp. 1–5.

[18] P. Ladoux, Y. Hachicha, D. Cypers, M. Meli, and N. Roux, "New method for determining the low-frequency stability limit of a 50 Hz electric traction power system," *Elektrische Bahnen*, vol. 10, no. 10, p. 18, Oct. 2020. [Online]. Available: https://hal-univ-tlse3.archives-ouvertes.fr/hal-03286350

[19] A. Yazdani and R. Iravani, *Voltage-Sourced Converters in Power Systems*. Hoboken, NJ, USA: Wiley, 2010.

[20] S. Golestan and J. M. Guerrero, "Conventional synchronous reference frame phase-locked loop is an adaptive complex filter," *IEEE Trans. Ind. Electron.*, vol. 62, no. 3, pp. 1679–1682, Mar. 2015.

[21] K. Ogata, *Modern Control Engineering* (Instrumentation and Controls Series). Upper Saddle River, NJ, USA: Prentice-Hall, 2010. [Online]. Available: https://books.google.es/books?id=Wu5GpNAelzkC

[22] Y. Zhou, H. Hu, X. Yang, J. Yang, Z. He, and S. Gao, "Low frequency oscillation traceability and suppression in railway electrification systems," *IEEE Trans. Ind. Appl.*, vol. 55, no. 6, pp. 7699–7711, Nov. 2019.

[23] X. Yuan, W. Merk, H. Stemmler, and J. Allmeling, "Stationary-frame generalized integrators for current control of active power filters with zero steady-state error for current harmonics of concern under unbalanced and distorted operating conditions," *IEEE Trans. Ind. Appl.*, vol. 38, no. 2, pp. 523–532, Mar. 2002.

[24] L. Buhrkall, "Traction system case study," in *Proc. IET Prof. Develop. Course Electric Traction Syst.*, 2008, pp. 53–71.

[25] G. Calzo, A. Lidozzi, L. Solero, and F. Crescimbini, "LC filter design for on-grid and off-grid distributed generating units," *IEEE Trans. Ind. Appl.*, vol. 51, pp. 1560–1639, Mar. 2015.

[26] S. Jayalath and M. Hanif, "Generalized LCL-filter design algorithm for grid-connected voltage-source inverter," *IEEE Trans. Ind. Electron.*, vol. 64, no. 3, pp. 1905–1915, Mar. 2017.

PAUL FRUTOS-GALARZA (Student Member, IEEE) received the B.S. degree in electrical engineering from the San Francisco de Quito University, Quito, Ecuador, in 2013, and the M.Sc. degree from the University of Nottingham, Nottingham, U.K., in 2017. He is currently pursuing the Ph.D. degree in electrical engineering with the University of Oviedo, Asturias, Spain. His research interests include control strategies for multilevel inverters, solid-state transformers, stability studies of high-speed railway systems, and the development of control strategies of power converters for traction applications.

JUAN M. GUERRERO (Senior Member, IEEE) received the M.E. degree in industrial engineering and the Ph.D. degree in electrical and electronic engineering from the University of Oviedo, Gijón, Spain, in 1998 and 2003, respectively. Since 1999, he has occupied different teaching and research positions with the Department of Electrical, Computer and Systems Engineering, University of Oviedo, where he is currently a Full Professor. From February 2002 to October 2002, he was a Visiting Scholar at the University of Wisconsin, Madison. From June 2007 to December 2007, he was a Visiting Professor at the Tennessee Technological University, Cookeville. His research interests include control of electric drives and power converters, electric traction, and renewable energy generation. He is an Associate Editor of the IEEE TRANSACTIONS ON INDUSTRY APPLICATIONS.

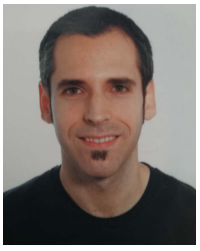

IKER MUNIATEGUI-ASPIAZU received the Industrial Technical Engineering degree (electronic design specialization) and the Industrial Automatics and Electronics Engineering degree from the University of Mondragon, Mondragon, Spain, in 2004 and 2007, respectively. In September 2006, he joined Ingeteam Power Technology (formerly TEAM), Zamudio, Spain, where he worked as a Control and Regulation Engineer, and he is currently a Control and Regulation Manager of the Traction Department. His current research interests include power converter and advanced control drives, modulation techniques, and railway research issues such as ac catenary stability and mechanical vibrations in drive trains.

IBAN VICENTE-MAKAZAGA graduated in electrical engineering from the University of Mondragon, Mondragon, Spain, in 2003, and the M.S. and Ph.D. degrees from the University of Manchester, U.K., in 2004 and 2009, respectively. He joined Ingeteam Power Technology (formerly TEAM), Zamudio, Spain, where he works as a Control and Regulation Engineer involved in railway traction control for trams, locomotives, and EMUs. His current research interests include power converters and advanced control drives, modulation techniques, machine parameters, and speed estimation techniques as well as railway research issues such as ac catenary stability and mechanical vibrations in drive trains.

AITOR ENDEMAÑO-ISASI received the Industrial Technical Engineering degree (electronic design specialization) and the Industrial Automatics and Electronics Engineering degree, from the University of Mondragon, Mondragon, Spain, in 1997 and 2000, respectively, and the Ph.D. degree from Heriot-Watt University, Edinburgh, Scotland, U.K., in 2003. In 2003, he joined Traction Department, Ingeteam Power Technology (formerly TEAM), Zamudio, Spain, where he has been a Control and Regulation Engineer, involved in several traction control design projects for trams, locomotives, and EMUs. His current research interests include power converter and advanced control drives, modulation techniques, and railway research issues such as ac catenary stability and mechanical vibrations in drive trains.

DAVID ORTEGA-RODRIGUEZ received the Licentiate degree in electric and electronic engineering from Universidad Pais Vasco of Bilbao (UPV), Spain, in 2004. He worked as a Development Engineer at the Traction Department, Ingeteam, from 2004 to April 2010. He joined Euskotren as a Rolling Stock Maintenance Engineer. Later in December 2010, he again joined the Traction Department, Ingeteam, where he is currently a Technology Coordination Manager. His research interests include rolling stock architectures, EMC, noise, efficiency, and high-power converters for traction and energy recovery systems.

FERNANDO BRIZ (Senior Member, IEEE) received the M.S. and Ph.D. degrees from the University of Oviedo, Gijón, Spain, in 1990 and 1996, respectively. He is currently a Full Professor with the Department of Electrical, Computer and Systems Engineering, University of Oviedo. His current research interests include electronic power converters and ac drives, power systems, machine monitoring and diagnostics, and digital signal processing. He received an IEEE Transactions on Industry Applications Award and nine IEEE Industry Applications Society Conference and IEEE Energy Conversion Congress and Exposition prize paper awards. He is the Past Chair of the Industrial Drives Committee of the Industrial Power Conversion System Department (IPCSD), IAS. He is currently the Vice Chair of IPCSD. He has served on scientific committees and as the Vice Chair or a Technical Program Chair for several conferences, including ECCE, IEMDC, ICEM, ICEMS, and SLED. He is a Member of the Steering Committee of IEEE JOURNAL OF EMERGING AND SELECTED TOPICS IN POWER ELECTRONICS. He is an Editor of IEEE Journal of Emerging and Selected Topics in Power Electronics and an Associate Editor of *IAS Transactions*.